Bacterial Social Networks: Targeted Delivery of Outer Membrane Proteins via Membrane Vesicle Chains

By

Jonathan Paul Remis

A thesis submitted in partial satisfaction of the
Requirements for the degree of

Master of Arts

In

Comparative Biochemistry

In the

Graduate Division

Of the

University of California, Berkeley

Committee in charge:

Kenneth H. Downing, Co-Chair
Fenyong Liu, Co-Chair
Bing K. Jap

Spring 2012

Abstract

Bacterial Social Networks: Targeted Delivery of Outer Membrane Proteins via Membrane Vesicle Chains

By

Jonathan Paul Remis

Master of Arts in Comparative Biochemistry

University of California, Berkeley

Doctor Kenneth H. Downing, Co-Chair
Doctor Fenyong Liu, Co-Chair

Despite the fact that most bacteria exist as part of multi-cellular biofilms in natural and pathogenic ecosystems, very little is known about the ultra-structure of their component cells, the precise arrangements of their community architecture or how they are able to communicate with each other. Using modern sample preparation and imaging methods we are able to see, with minimal artifacts, a more accurate representation of the organization of such communities. Cells of the social soil bacterium *Myxococcus xanthus* displays a variety of complex and highly coordinated behaviors, including a social form of motility, group predation, outer membrane protein transfer and fruiting body formation. Here we show that these cells have the ability to form lipid vesicles as well as continuous outer membrane extensions in the form of fused vesicle chains and lipid tubes that may be important in intracellular communication. We have shown that these lipid structures contain membrane proteins known to be transferred between cells in a contact-dependent manner and are produced in much greater amounts in a biofilm when compared to planktonic cultures. Most significantly, we have imaged individual cells in the biofilms connected via an extensive network of these membrane extensions that may connect the cells of the biofilm at the level of the periplasmic space. Such a network would allow the transfer of membrane proteins between cells, and likely represents the mechanism for cell-cell communication.

Introduction

Recent decades have seen a profound change in our concepts of the growth of bacteria in both natural and pathogenic ecosystems, in that the notion of groups of individual planktonic cells has given way to the concept of integrated microbial communities. Unlike their much more studied and better-understood planktoniclly living counterparts most bacteria actually exist in biofilms (1). In this type of environment the cells exist surrounded by other bacteria attached to a solid surface and tend exhibit an entirely different protein expression pattern from those of free floating single cells (2). Within a biofilm, bacteria are typically embedded in an extracellular polymeric substance (EPS) matrix (3,4,5) that protects the microbial community members from desiccation, from phagocytosis, and, in the case of human pathogens, from the host immune system (6).

Transmission electron microscopy is a nearly ideal method to study the precise arrangement of these biofilms because of the ability to section through thick samples and image the internal arrangements at high resolution. The details observed by such imaging techniques are only useful to us though if we can be sure that we are not merely imaging artifacts caused by the sample preparation itself. Only a few biofilms have been faithfully preserved and visualized at high resolution by transmission electron microscopy (7, 8, 9, 10, 11, 12, 13). A recent ultra structural study of *Pseudomonas aeruginosa* biofilms shows that high-pressure freezing/freeze-substitution results in superior preservation (**8**). Unlike conventional sample preparation, millisecond cryofixation and low-temperature dehydration protocols minimize artifacts from chemical fixation, extraction, and aggregation (14, 15, 16, 17, 18). Attempting to draw sound conclusions based on data filled with artifacts can have dire consequences.

Our model system for studying the interactions of cells within a biofilm is that of the social bacteria *Myxococcus xanthus. Myxococcus xanthus* is a well-studied gram-negative soil scavenger and predator, moving over surfaces either as a single cell by adventurous (A) motility or as a group using social (S) motility (19). It forms spore-bearing fruiting bodies upon starvation, in a process that requires the coordinated movement of many thousands of cells. It is also well documented that outer membrane proteins can be exchanged between cells in the biofilm though a process known as stimulation(18). One of the things that intrigued us most was exactly how do bacterial community members interact with one another and what mechanisms they employ for effective communication and signal and/or material transfer in such crowded busy communities sometimes containing multiple species.

We have shown that cells produce large numbers of vesicles, to which we (20) and others (21) have ascribed the possibility of ability to transfer membrane proteins that stimulate S-motility in cells that lack the genetic capability for this social activity. Recently Dubey and Ben-Yehuda-(21) have shown that cytoplasmic contents, including non-conjugative plasmids, may be transferred via bridges between cells of *Bacillus subtilis,* between *B. subtilis* and *Staphylococcus aureus*, and

even between *B. subtilis* and the distantly related cells of *Escherichia coli*. Recent work by Wei et al. (23) shows intercellular outer but not inner membrane lipoprotein transfer, but does not provide a mechanism. Independent work has examined the structure and function of the intercellular "nanowires" to which Gorby et al.(24) and Lovely et al.(25) have attributed the ability to carry electrical currents between cells within biofilms. Observations of nanowires and nanotubes by scanning electron microscopy (SEM) are complicated by eutectic drying artifacts, (26) such that controversies have arisen concerning both their structure and their very existence (27). A recent study by Dohnalkova et al.(28)attributed intercellular linkages, often found in SEM images of bacteria, to critical point drying artifacts of EPS. Observations of these structures by transmission electron microscopy (TEM) are complicated by the small volume of ultrathin sections typical for TEM imaging, making it virtually impossible to follow such extracellular extensions from cell to cell. Thicker sections suffer from the superposition of structures in projection images precluding an unambiguous identification of such cell-to-cell connections. We have undertaken this study to apply virtually artifact-free, ultra-rapid freezing preparative methods, and advanced 3D electron microscopy imaging techniques that overcome these previous limitations.

We first observed the intriguing lipid tubes that *Myxococcus xanthus* produces when using a TEM to image sections of resin embedded and stained dense biofilms. The sections were cut so that the cells could be observed in a direction where the cells were primarily in longitudinal orientation. This was somewhat easy to do as the cells naturally align with each other and the rod-shaped cells always lie flat on the surface that they are gliding across. The abundance of these outer membrane derived extracellular membrane extensions in the form of vesicle chains, constricted tubes and uniform tubes made them impossible to miss but nevertheless surprising. We also imaged cells grown under shaken planktonic conditions and noticed that although most of the cells that had no lipid structures attached some still did. Being able to image single cells as opposed to entire colonies provided us with the opportunity to use a few microscopy techniques that we wouldn't be able to apply to crowded biofilms. Techniques such as low dose TEM imaging of unstained frozen cells, whole mount negatively stained TEM imaging and light microscopy of single moving cells were all necessary to complete this study.

Tomography of biofilms:

By imaging the same areas of a *M. xanthus* biofilm by 2D projection and by 3D tomography, a side-by-side comparison as seen in Fig. 1 illustrates the improvement of resolution in the *z*-axis provided by using 3D tomography. A 250 nm section was taken of a biofilm grown on Isopore filters with bacteria oriented longitudinally (Fig. 1A and B). These images display the long rod shaped cells and the structures of both the cytoplasm and what we believe to be the chromatin body (*). The cells in this particular section are not densely packed, vesicles in the extracellular space can

be readily visualized. Figure 2A is a projection view while 2B is a ~1nm slice through a tomogram of the same region. Figure 2C and D show a densely packed biofilm grown on cellulose tubing visualized in a cross-sectional orientation. Cellular features obscured by superimposition in two dimensions are resolved in the third dimension in the tomogram, allowing 3D visualization and feature extraction. Asterisks denote chromosomal DNA, and arrows point out the biofilm boundary.

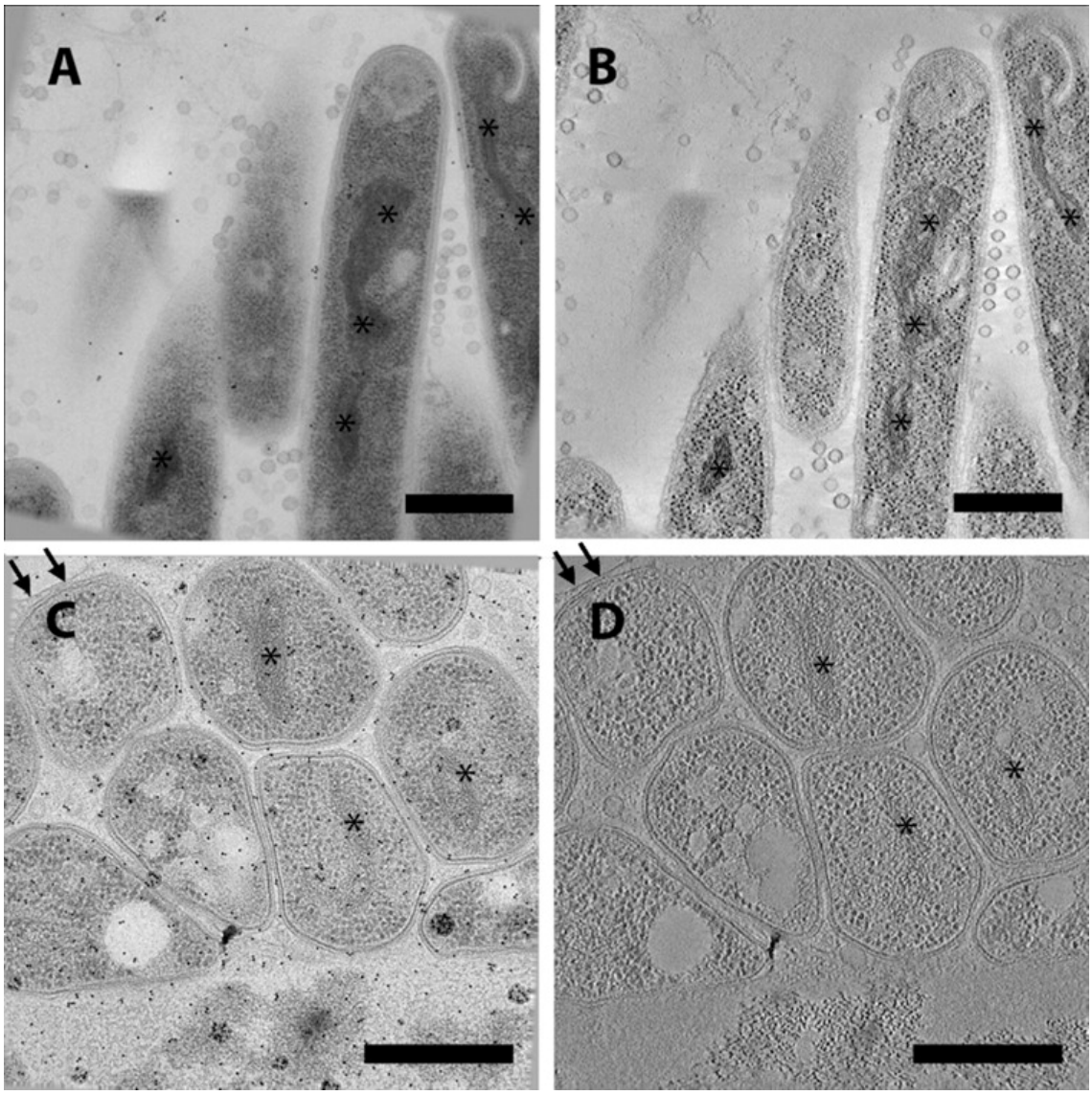

Figure 1: TEM analysis of high pressure frozen resin embedded *Mxyococcus xanthus* biofilms. Projection images are compared with imaged obtained from reconstructed tomograms. **(A**) Lengthwise and **(C)** cross section 2D projection images. **(B,D)** corresponding virtual sections from tomograms obtained in identical samples in figure a and c. (*) Denotes chromosome. **(Arrow)** shows the top boundary of the biofilm. All scale bars are 0.5 micron

Intracellular features:

At the center of the bacteria we detected high-contrast multi-stranded filamentous densities resembling a twisted closed circle that often showed prominent clefts along the longitudinal axis (Fig.2A-C). We interpret the entity of these filamentous densities as the bacterial chromosomal DNA. Interestingly, and particularly obvious when viewed in cross-section, we typically found the chromosomal DNA at the center of the cell, independent of whether or not the cell is in intimate lateral contact with its neighboring cell. Therefore, even in such close contacts (see below), there is no structural evidence of chromosomal DNA exchange, although the exchange of small portions cannot be excluded. In the reconstructed volumes, strands that we consider to be DNA were ~3 to 5 nm thick**.** We also observed two types of intracellular organelle-like features. While detectable in 2D projections, the characteristic shapes of those intracellular structures became obvious only by 3D tomographic reconstruction. These membrane-delineated features resemble organelles and are either of crescent (Fig. 2D) or concentric spherical (Fig. 2E) shape. The intermembrane space in the crescent-shaped compartment, as well as the sphere-like organelle, is bridged by filaments that, given their staining properties, are likely to be proteinaceous in nature. Interestingly, ribosomes or similarly sized macromolecules are excluded from the cytoplasmic space enclosed by the rings. The function of the sphere-like and the crescent-like features remains elusive. Being able to purify these structures and make a GFP mutant where the labeled protein preferentially localized to these structures may prove useful for live cell assays. The mechanism for single celled movement, adventurous motility, is not understood and maybe these structures play an important role. Also important to note is that after imaging at least 20 samples these structures were almost never found in cells grown planktonicaly only in cells living in a biofilm.

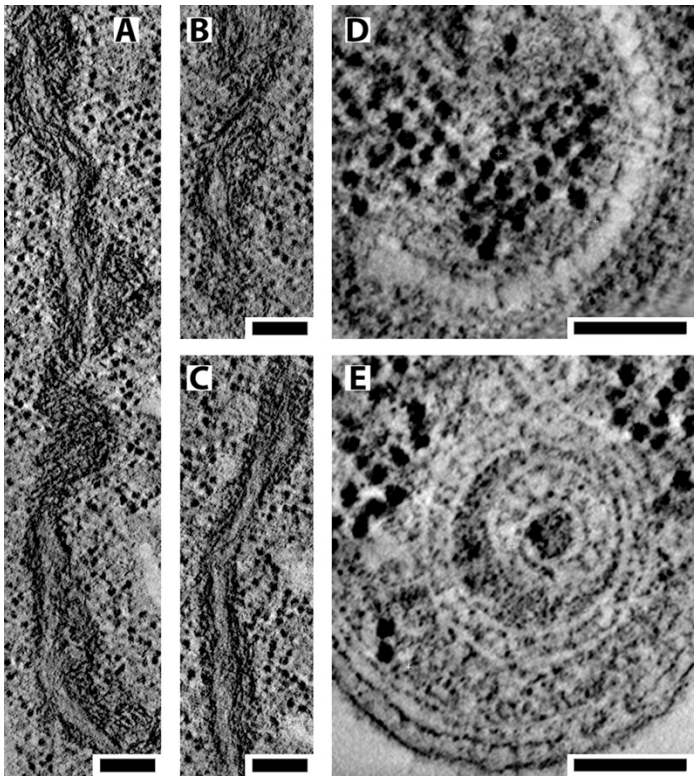

Figure 2: Virtual sections taken from high magnification TEM tomograms showing showing intracellular structures. **(A-C)** chromosomal DNA is easily recognizable due to its high contrast and strand-like appearance. **(D)** Crescent-shaped membranous structure. **(E)** Cocentric ring-shaped organelle. Scale bar throughout figure is 100nm.

Biofilm vesicles:

In both thin and thick *Myxococcus* biofilms, the extracellular space is filled with vesicles with a diameter of 30 to 60 nm (Fig. 3). It should be emphasized that in our cryo-immobilized samples we did not observe signs of cellular stress and cell disintegration due to their nearly instant freezing procedure. The membranes on these cells are smooth, unlike what is often found in chemically fixed samples, where membranes often display blebbing and other artifacts. We are so confident in this sample preservation that we interpret the indentation in the bacterial membrane (Fig 3A) to suggest either a recent or soon to be endo- or exocytosis event. Often, the 3-D reconstruction revealed that bacterial vesicles were either directly in contact with bacterial membranes or linked to cell membranes by what appear to be tethers (Fig. **3**B, D, and E). Occasionally, a vesicle was seen in direct contact with three bacterial cell membranes (Fig. 3C). Vesicles were found tethered not only to the bacterial outer membrane surface but also to each other (Fig. 3D and

E). The tethers appear as short filaments of about 3 nm in diameter and tens of nanometers in length. On the surface of a number of vesicles we find protrusions that are likely to be integral membrane proteins. The scale Bar is 100 nm for the entire figure.

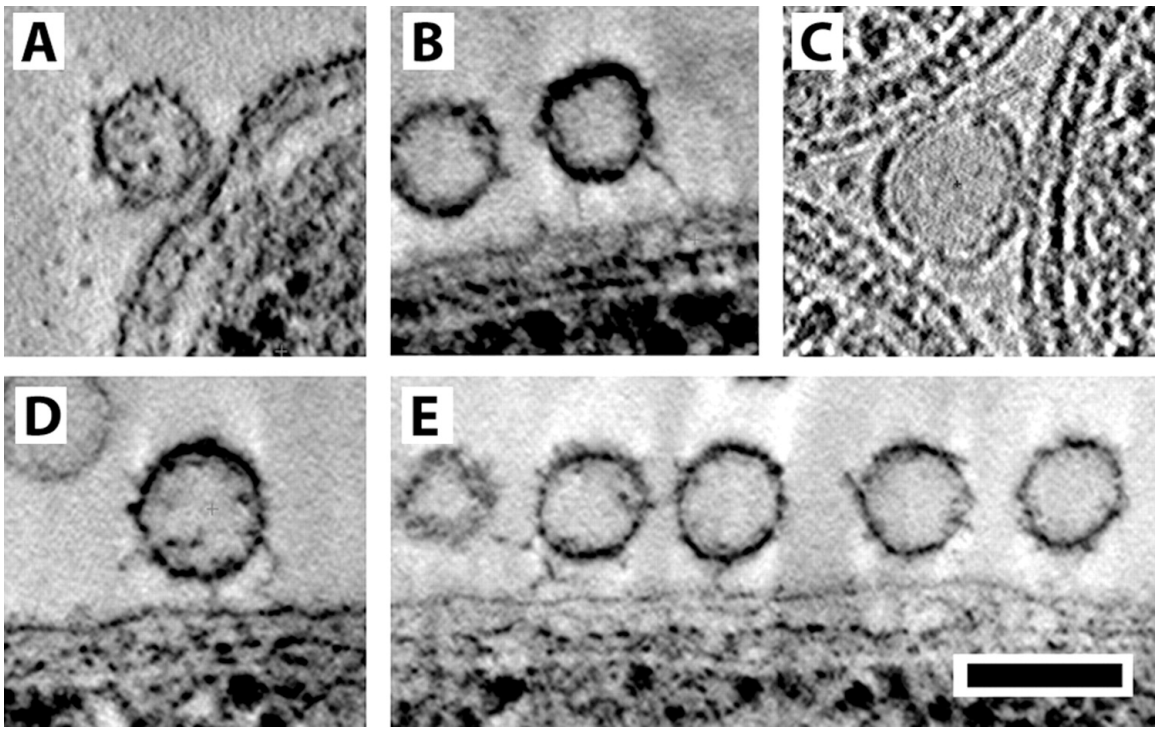

Figure 3: Ultrastructural characterization of vesicles and cell–cell contacts in high-pressure frozen and freeze-substituted *Myxococcus xanthus* biofilms. **(A)** The indentation in the bacterial membrane may suggest either an endo- or exocytosis event. (**A,B** and **D**) The vesicle interior displays densities that are indicative of either the presence of a cargo or an underlying protein organization. The vesicle is tethered to the membrane by at least one or two links of unknown composition. **(C)** Occasionally, vesicles were found in simultaneous contact with three bacterial outer membranes. **(E)** Five vesicles shown in linear arrangement close to the bacterial cell surface. Scale Bar, 100 nm.

High resolution TEM and analysis of the extracellular lipid structures

Descriptions of extracellular membranous structures such as nanotubes always hinge on preservation, because membranes are notoriously difficult to preserve faithfully during chemical fixation, and require high resolution imaging as their dimensions lie beyond the limits of optical microscopy. We verified, unequivocally, the *in-vivo* presence of lipid-based extracellular appendages using epifluorescence light microscopy of lipophilic FM4-64 labeled single cells (Fig. 4A).

We have confirmed these findings using ultra-rapid freezing (cryofixation) followed by cryo-TEM projection imaging (Fig. 4B,C) of whole-mounted individual bacteria, cryo-tomography of biochemically isolated vesicle chain whole-mount samples (Fig 4D), room-temperature electron tomography of resin-embedded biofilm resin sections (Fig. 4E), and negative-stain whole-mount TEM projection imaging (Fig. 4F). We found chains of vesicles that were connected to one another but not fused, displaying a remarkably uniform size within each chain, whereas the vesicle diameter ranged from 30 to 60 nm between different chains (Fig. 4B,D). Furthermore, we also found tubular structures that were either of uniform dimensions (Fig. 4C) or periodically constricted (Fig 4 E,F). Interestingly, we could not detect any external protein machinery at such sites of constriction, suggesting that these are either regulated within the membranes or possibly through luminal proteinaceous structures. Clear distinction of the type-IV pili extending from the cell pole (Fig. 4b) indicates faithful preservation and high image quality. In the cryo-preserved samples the membranous surface of both the cell and the appendages displayed short hair-like protrusions that were not visible in stained samples, suggesting that such structures are composed of carbohydrates, which are known to stain poorly with heavy metals, and presumably represent the lipopolysaccharide (LPS) O-antigen side chains. Vesicle chains and tubes were found both in planktonic cells (Fig 4a, b, c, f) and in biofilms (Fig 4d, e), but were present in much larger numbers in the latter mode-of-growth

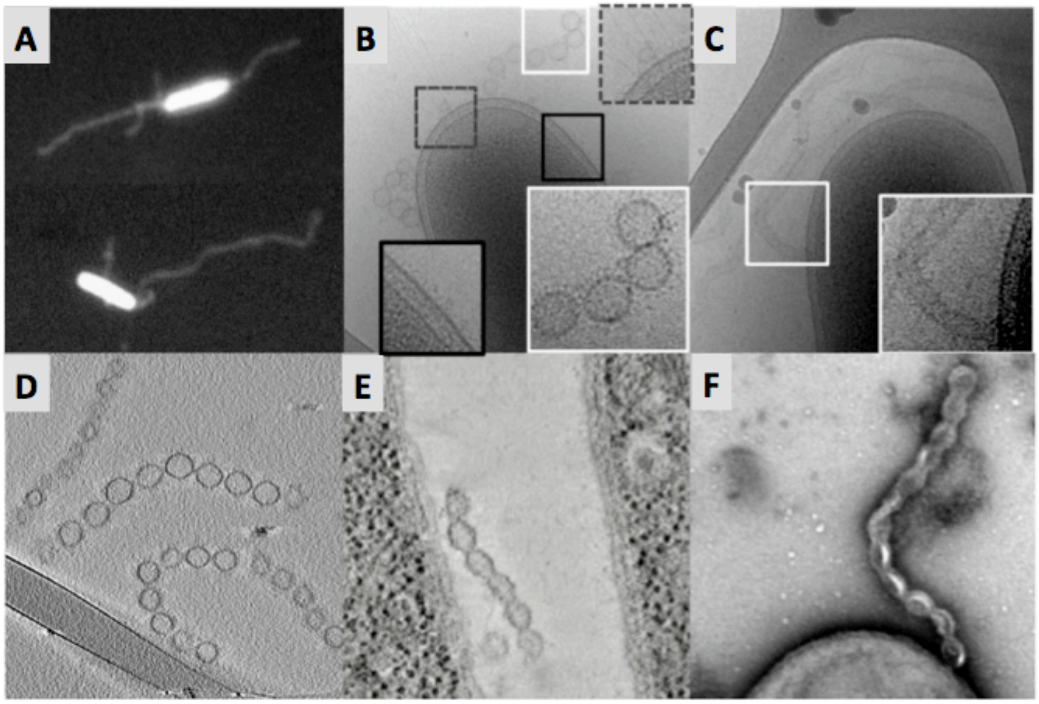

Figure 4: The vesicle chains are seen as long extracellular appendages **(A)** when living cells are stained with the lipid bilayer dye FM4-64 and visualized by epifluorescence light microscopy. These lipid structures are resolved as vesicle chains/tubes **(B** and **C)** when cryofixed and visualized by transmission electron

microscopy, and the lumen of the extensions can be seen to be continuous in some cases **(C).** These fast-frozen, artifact-free, preparations show how each chain is made up of vesicles of the same size whereas vesicle size can differ between different chains **(D)**. A 1 nm thin slice through a 3D tomogram of a HPF/FS, resin-embedded sample **(E)** and a negatively stained whole-mount projection image **(F)** reveal a continuous lumen inside the constricted vesicle tube **(E).**

Gliding motility and the potential role of the vesicle chains.

After a thorough literature search it became clear that at a very low resolution view of these structures they have superficial similarity to the so-called "slime" and "fibrils" described by Kaiser and colleagues and Shimkets and colleagues, respectively(29, 30, 31, 32). We set out at first to test whether these structures that we imaged had any of the properties attributed to "slime" and "fibrils", that is they are not needed for adventurous motility and not present on fibril mutant cells. If these appendages did not share the same functional properties as the two proposed in the literature we may have found a structure with new properties not described. Conveniently having a lipid component themselves, the lipid structures stained with dye FM4-64, a hydrophobic dye that only fluoresces when it is in the center of a bilayer. Despite their apparent similarity to the so-called slime described by Kaiser and colleagues the extracellular appendages described here do not correlate with A-motility as only a small fraction of all moving cells display such trailing appendages (Fig. 5A-E). This portion of the figure shows images every 90 seconds taken from a movie of moving cells stained with FM4-64. On the final frame of the movie (E) fluorescent imaging settings are used and the location of the stained lipid structures are revealed. If not all moving cells have lipid tails then a protruding lipid or slime tail cannot be the mechanism for motility. The dye is so sensitive and our microscope is sensitive that if cells somehow pushed themselves forward using these structures we would certainly have seen trailing fluorescent densities behind every moving cell. While our extracellular membrane structures ultrastructurally resemble the so-called fibrils unlike the fibril controls prepared according to Yu and Kaiser (30) our highly purified fractions neither promote cell clumping nor do they result in type-IV pilus retraction. We do note that N-acetylglucosamine (GlcNAc), a carbohydrate moiety which is associated with pilus retraction (33) is both present and accessible on the cell surface and the extracellular appendages, as evidenced by wheat-germ agglutinin binding(5F and G), as well as liquid chromatography mass spectrometry (data not shown) and FACE gel carbohydrate analysis (H) (ref 34).

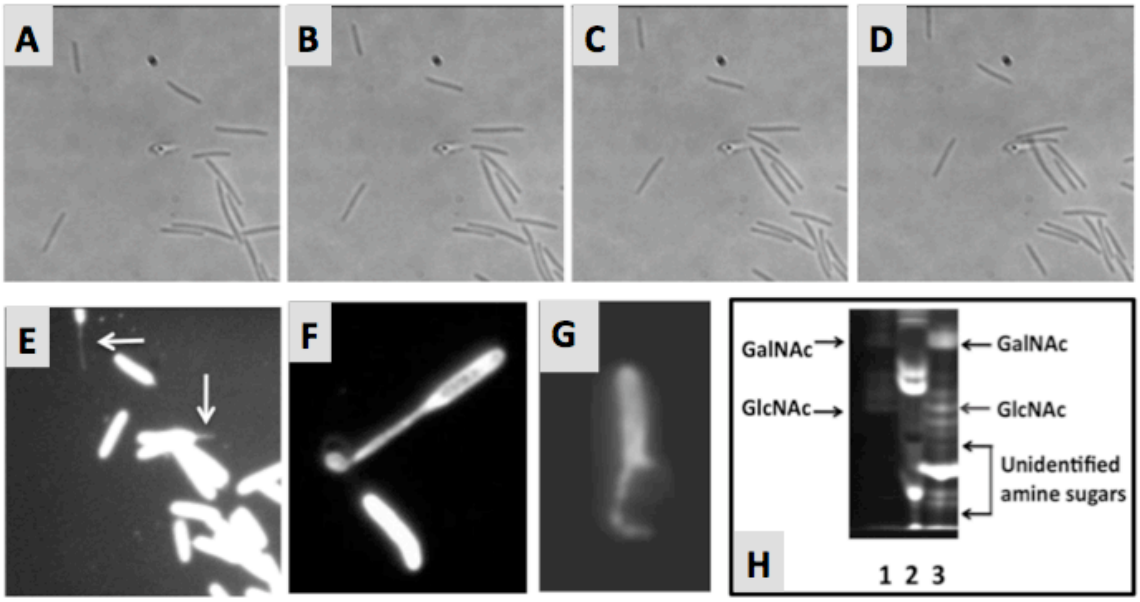

Figure 5: Time-lapse phase contrast microscopy of *M. xanthus* cells gliding on hard agar for 0, 45, 90, 135 seconds, respectively (**A-D**). After a total of 180 seconds lipophilic dye FM6-46-loaded cells are imaged by fluorescence microscopy, revealing that only a fraction of the moving cells display a membrane tail (**E**). WGA conjugated fluorophore stained both WT (**F**) and EPS- (**G**) cells. FACE analysis of acid-digested purified vesicle chains revealed the presence of the monosaccharide GlcNAc.

The abundance of extracellular lipid structures depends on local environment

All of our imaging data indicated that these appendages, while present in planktonic cells, seemed to be up-regulated in biofilms where they filled nearly every possible free extracellular space. The physical contact and interactions between bacterial cells is influenced by their local environment and how they are cultured. So after normalizing for total cellular mass , the amount of vesicle structures produced was compared between samples of cells grown planktonicly to different densities with that of cells grown in biofilms for different amounts of time. As expected it was found that the amount of extracellular membrane structures, as measured by lipid fluorescence of cell free purified sample, to be higher in biofilms compared to planktonic cells as shown in Fig 6A but the planktonic density or age of biofilm had little to do with it. The purified sample was inspected by TEM and quantification of isolated and purified vesicle chains and tubes (Fig 6A,B,C) was compared between planktonic cultures grown at different densities and biofilms. Small groups of cells from biofilm samples often display many such extracellular membrane assemblages even after re-suspension in medium (Fig. 6D,E). We further noticed that such membrane structures are often found in faithfully preserved biofilm samples and are clearly visible by TEM of thin sections (Fig 6f).

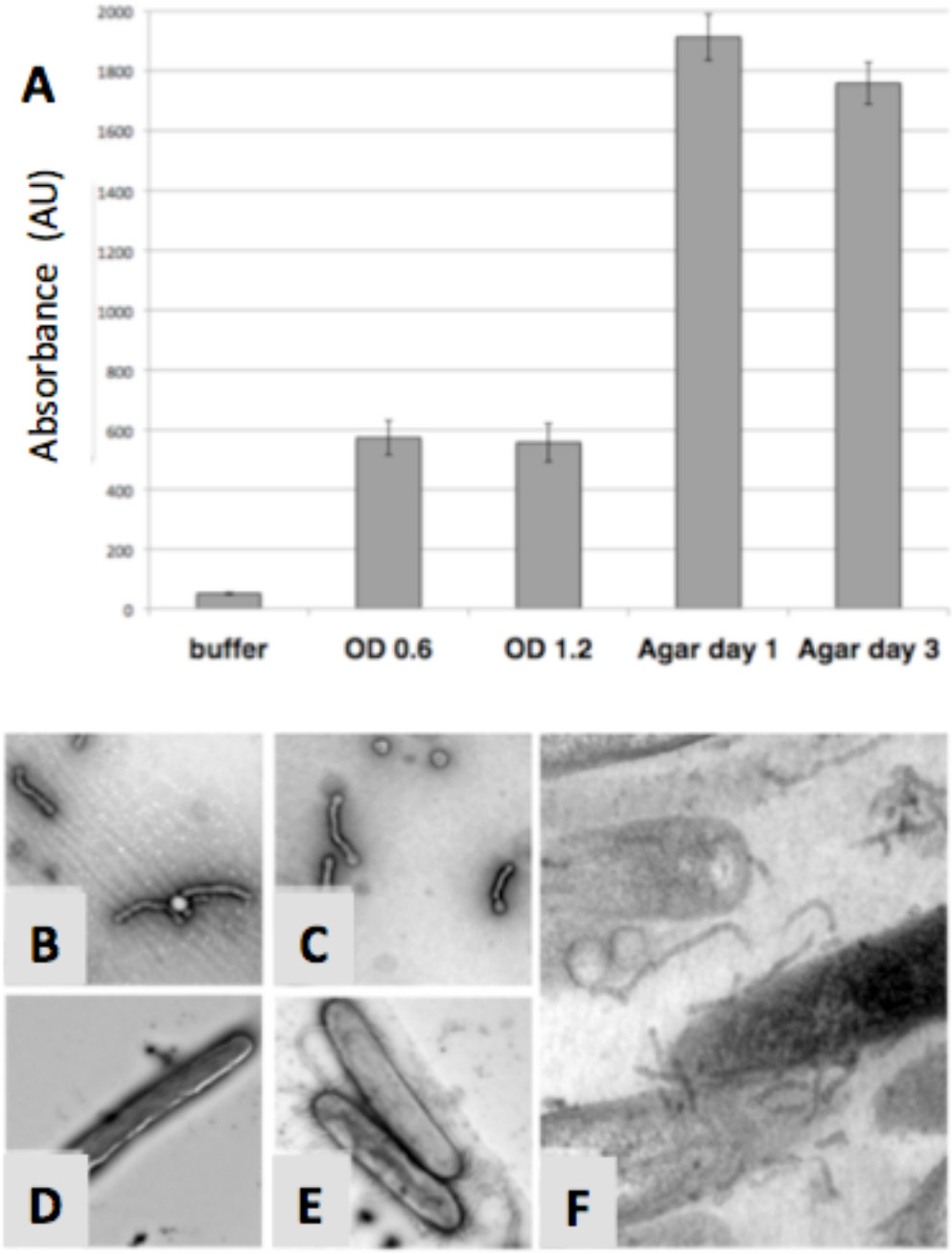

Figure 6: Vesicle chains were purified from planktonic cell cultures or biofilm communities grown on nutrient rich agar plates. After cell mass normalization we quantified FM4-64 intensity to determine membrane structures concentration **(A).** Aliquots of purified vesicle chains from both planktonic cell cultures **(B)** and biofilms **(C)** were examined by whole mount TEM to exclude cell membrane contamination. Negative staining of individual *M. xanthus* cells fresh from culture solution reveals that such cells rarely show vesicle chains **(D)**, whereas cells

resuspended from biofilms frequently show many vesicle chains **(E).** Vesicle chains are frequently observed in *M. xanthus* biofilms as revealed by TEM imaging of ultrathin biofilm sections **(F).**

Proteins of Interest Identified in the Membrane Vesicle Protein Extract.

Because of the major difference in size between the vesicles and related lipid structures and bacterial cells the two were easily separated. Biofilms were vortexed to try to get as much of the extracellular material freely floating in suspension as possible. The large mass difference allowed us to centrifuge the suspension of cells and vesicles at low speeds (10000xG) for 10 minutes and have only the cells sediment to the bottom of the tube while leaving the vesicle fraction in solution. The supernatant and was then filtered through 0.45 micron and then 0.22 micron filters allowing the smaller vesicles that were around 50nm diameter to pass through. The extracellular lipid fraction could finally be pelleted by centrifuging at high speeds (100000xG)for 2 hours. The protein extract was run on an SDS-PAGE gel and bands cut out and subjected to in-gel digestion followed by LC-ESI-MS/MS and identification of proteins by database searching. 78 unique proteins were identified and depicted here (figure 7) on an illustration of the *Myxococcus xanthus* chromosome.

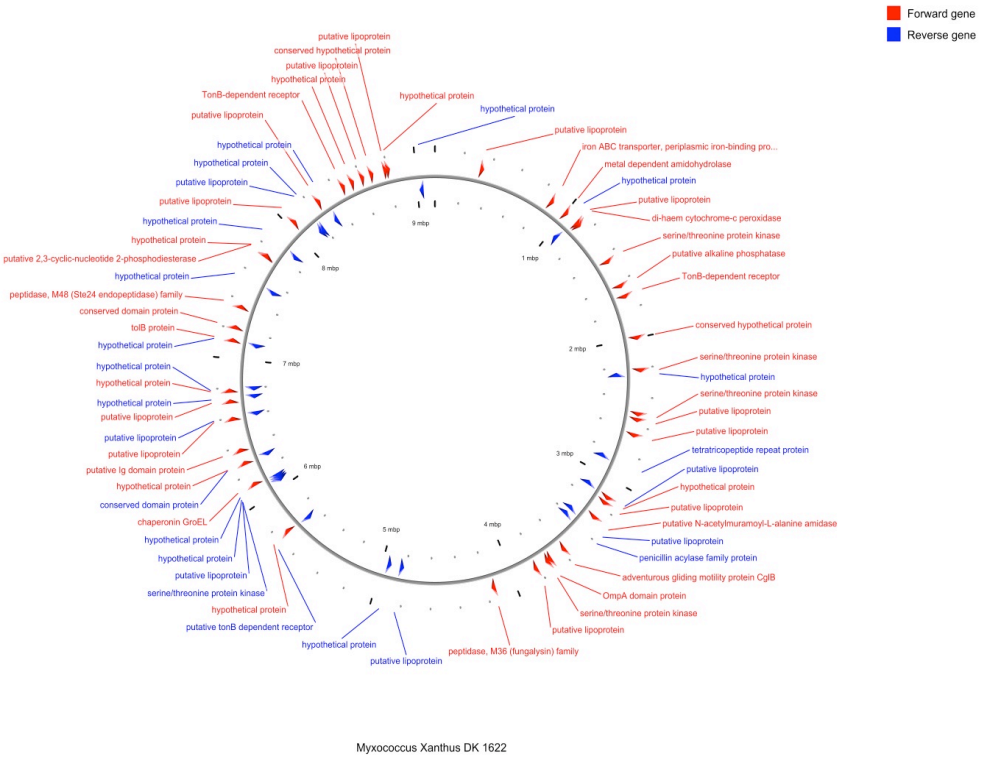

Figure 7: Proteins found in the extracelluar lipid fraction displayed on the *Myxococcus xanthus* chromosome.

Out of all of the proteins identified we hope that some of them are essential for vesicle formation. A systematic mutational analysis is currently underway knocking out each of these proteins to determine if one or more of them is necessary for vesicle formation. If we do find a mutant that lacks vesicles and lipid structures it will be of great interest to see what other phenotypes this mutant has and may lead us to better understand the function of these vesicles and tubes. Two of the proteins that were of great interest to us were a 45kd outer membrane protein, CglB and a 28kd outer membrane protein Tgl. Both of these proteins had been shown to be transferable in the biofilm and are contained in the vesicle fraction and indicate that maybe these structures can be used as a vehicle for protein transfer between cells. It is not known how many other proteins are transferred between cells because the assay for stimulation only detects motility proteins. Because of the sensitivity of mass spectroscopy we are currently doing antibody labeling experiments to rule out protein contributions caused by contaminating outer membrane fragments.

Extensive Intercellular Membrane Network in Biofilms.

We had hypothesized that these lipid extensions could form stable connections between cells in the biofilm but our traditional TEM methods wouldn't allow us to trace these potential bridges. TEM imaging of thin sections typically does not allow tracing/mapping of such membrane tubes and vesicle chains to their respective ends. To overcome both the shortcomings of ultrathin-section TEM imaging we have used a novel method for true 3D imaging of resin-embedded samples, known as Focused Ion Beam Scanning Electron Microscopy (FIB/SEM) (35). In short, the surface of a stained embedded sample block is imaged with SEM, then an ion beam burns away a uniform "step" from the sample block and the face is imaged again. This process takes place hundreds of times and the images are then stacked ontop of one another to create a three-dimensional image. We were able to image a volume of up to 10 micrometer by 8 micrometer by ~15 micrometer at XY pixel scanning size as small as 2 nm and a Z interval of 5 nm. Our novel analysis of large volumes of biofilms (fig 4) allows us to conclude that these structures constitute a ramifying network that connects virtually all of the cells in a biofilm, often by multiple connections (fig 4E), to form a very large syncytial community. These vesicular connections intercellular bridges that may have the capability of transferring information or materials cells thus enabling biofilms of this bacterial species to function as a dynamic multi-cellular organism. The recent demonstration(36) that cells of *B. subtilis* can exchange cytoplasmic constituents with each other and with cells of different species, via nanotubes of undefined structure, suggests a functional role for the network we have described in *M. xanthus* biofilms. Sanchez (36) has pointed out that this newly discovered cytoplasmic continuity between cells in a

microbial biofilm community links the eubacteria to higher plants and animals that use plasmodesmata and desmosome complexes (respectively) to produce similar multicellular syncytia.

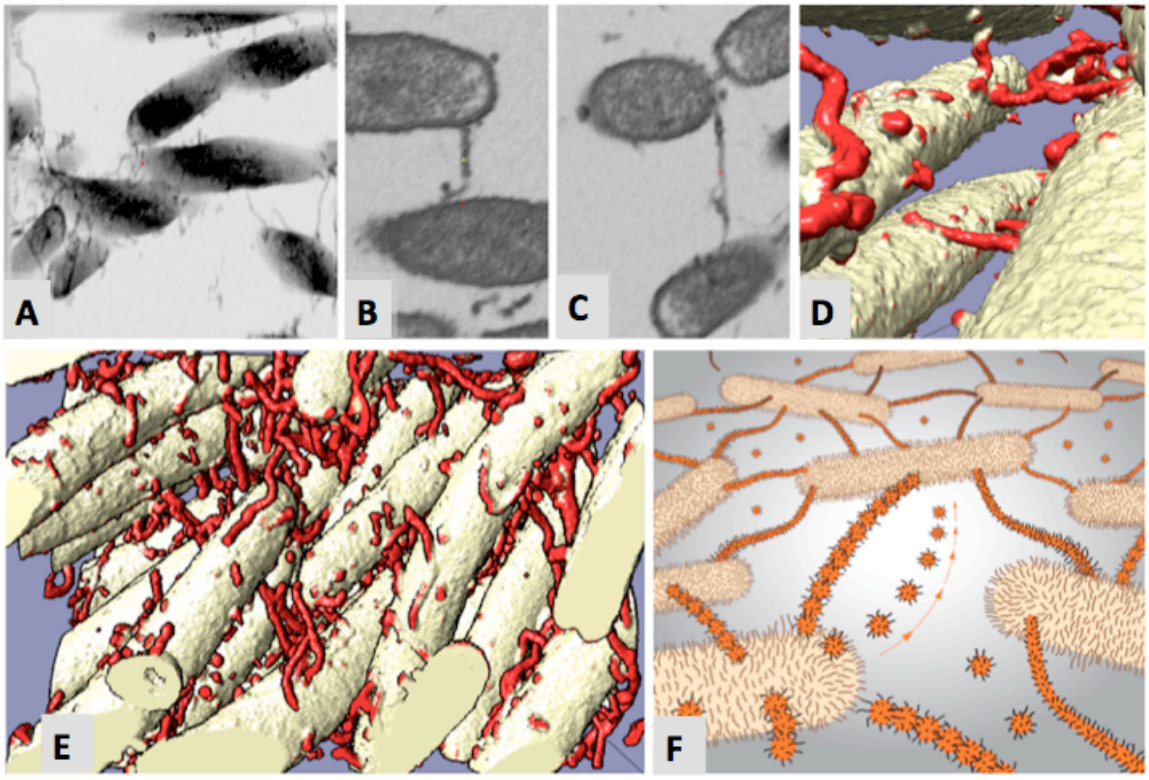

Figure 8: Macromolecular resolution 3D FIB/SEM imaging of faithfully preserved large volumes of *M. xanthus* biofilms reveals the abundance of vesicle chains and tubes **(A-E).** A ~500 nm thick slice through the reconstructed 3D volume reveals that each cell is linked to their neighboring cells through multiple membrane connections **(A).** Such connections can be vesicle chain-like **(B)** or tubular **(C)** in nature and these membrane-based structures mediate cell-to-cell connectivity **(B, C).** Surface rendering of the 3D volume **(D,E)** shows the high frequency of such connections (shown in red) between neighboring cells (shown in beige) in a ~8 micron thick volume of *M. xanthus* biofilm. We have constructed a model **(F)** illustrating the vesicles, vesicle chains and fused-vesicle tubes that M. xanthus uses to produce the network of intercellular structures that connects virtually all of the cells in a biofilm to form a functional syncyticum

Discussion and Conclusions

Although the lipid vesicles and vesicle chains and tubes may have multiple functions we believe that one of them is a mechanism for material transfer in between cells in the biofilm. The membrane-based network we have discovered in *M. xanthus* has physical properties that differ from the much more rigid pili and, which have been proposed to mediate such processes as conjugation (37) in biofilm communities. In contrast to the open self-assembled protein structure of pili, membranes provide a fluid bridge between cells, within which individual proteins and hydrophobic molecules can move laterally in a sea of phospholipids, and thus form a dynamic continuum throughout the community. Membranes also define a fluid-filled space, with a barrier of variable permeability so that a tubular array of membrane bound vesicles constitutes a fluid-filled conduit connecting the periplasmic spaces of a large number of cells. Lipid vesicles existing as individual free floating structures could perform the same function potentially for long range communication. In order to examine whether our membranous structures have the potential to mediate this putative exchange of membrane-associated proteins, we have analyzed the proteome of vesicles, chains and tubes produced by strains of *M. xanthus* and found they contain CglB and Tgl proteins, known to be directly transferable between cells in a contact-mediated manner. CglB was also found in the vesicle fraction by Kahnt and colleagues, (21) and their work supports our proposition that vesicle secretion and fusion may be one of the underlying mechanisms of stimulation. It is interesting to note that adjacent cells have been shown to exchange signals via vesicles in *Pseudomonas* (38). Here we present supporting data and propose a mechanism for membrane-associated protein transfer through nanotubular lipid structures. In a scientific discipline as fluid as modern Microbiology, in which concepts of the basic mode-of-growth are moving from planktonic cells towards integrated sessile communities, we must mobilize new technologies as they become available and assemble the resultant data with rigor and an open mind. Because we have access to modern artifact-free cryo-preservation, combined with advanced 3D FIB/SEM imaging, we can both preserve and visualize structures that have been destroyed or blurred by previous methods. Combining these static techniques with live cell assays will provide an amazing amount of useful data to answer some of these bigger questions in microbiology. Unfortunately in our case, stimulation only occurs in dense biofilms so imaging a fluorescently tagged protein hop from one cell to the next through a lipid tube is not technically feasible. Even with the most advanced confocal microscopes, the contributing signal from nearby cell membranes would obscure the one rare event we want to witness. So we are left with a structure heavy argument in the structure-function world describing chains of vesicles and nanotubes that form an extensive network connecting virtually all the cells of a *Myxococcus* biofilm in a functional continuum. Hopefully in the near future a new method can be developed that allows real time monitoring of molecular exchange between cells and then without a doubt the mysterious function of the vesicle chains will be known.

Materials and Methods

Cell growth and mutants:
Myxococcous xanthus DZ2 (wild type) or DZ2 delta PilA cells were grown in liquid culture shaking at 200 rpm, 32 degrees Celsius in CYE media, consisting of 5 mM MOPS pH 7.6, 2 mM MgSO4, 0.5% (w/w) Bacto Casitone, 0.25% (w/w) Bacto Yeast Extract or on 1.5% agar plates with the same components. To grow biofilms on Cellulose microdialysis hollow fibers (Spectra/Por; Spectrumlabs, CA) or 1- by 1-mm^2 squares of Isopore membrane filters (HTTP, 0.4 μm; Millipore, MA), dense planktonic culture of cells was plated onto the substrate ontop of agar and were allowed to mature for 2-4 days before further experimentation.

High-pressure freezing and freeze-substitution:
Bacterial biofilms on microdialysis tubing or Isopore membrane filters were briefly immersed in 10% glycerol or 20% bovine serum albumin in CYE medium. Filters or tubing was transferred into 200-μm-deep type A aluminum planchettes that were sandwiched against the flat sides of type B planchettes. The specimens were cryofixed in a Bal-Tec HPM010 high-pressure freezer (2,100 bars, 5 to 7 milliseconds) (Bal-Tec, Inc., Carlsbad, CA). Using the Leica automated freeze-substitution system AFS (Leica Microsystems, Vienna, Austria), cryofixed specimens were freeze-substituted in anhydrous acetone containing 1% osmium tetroxide and 0.1% uranyl acetate and infiltrated with Epon-Araldite following established protocols (**39**). Specimens were flat-embedded between two microscopy slides and polymerized at 60°C over 1 to 2 days (**40**). Resin-embedded biofilm samples were remounted under a dissecting microscope for precise orientation.

2D projection transmission electron microscopy for sample surveying:
Thin (70- to 100-nm) sections were collected on Formvar-coated slot grids and poststained with 2% uranyl acetate in 70% methanol followed by either Reynold's or Sato's lead citrate. The sections were imaged in an FEI Tecnai 12 transmission electron microscope (FEI, Eindhoven, The Netherlands) or a Zeiss 10 instrument, operated at 120 kV or 80 kV, respectively. These samples were used for ultrastructural evaluation as well as to assess the quality of fixation for the tomography studies described below.

Whole mount TEM:
Negative stained TEM samples were prepared by applying the subject to 200 mesh formvar coated TEM grids (ted pella) rinsing briefy in distilled water before applying a 2.0% solution of Uranyl acetate before blotting off and air drying. Samples were imaged on a FEI CM200 microscope with a 2k x 2k Gatan CCD camera.

Cryo-TEM:
For cryo-electron microscopy (cryo-TEM) cells were placed onto lacey carbon grids (Ted Pella 01881) that were pre-treated by glow-discharge. The grids were blotted

and plunged into liquid ethane using a Vitrobot (FEI automated vitrification device) before being transferred and stored in liquid nitrogen until imaged. Images were acquired at 20,000 magnification on a JEOL–3100 electron microscope with an underfocus value of 10µm. The microscope is equipped with an FEG electron source operating at 300 kV, an Omega energy filter, a Gatan 795 2K x 2K CCD camera and cryo-transfer stage. The stage and sample were cooled to 80 K for the duration of data collection.

Electron microscopy tomography:

For tomography, thin sections (<100 nm) were imaged in a Tecnai T20 LaB6 instrument operated at 200 kV (UCSF), and semithick (200- to 300-nm) sections were imaged in an FEI Tecnai F30 microscope operating at 300 kV (Boulder Laboratory for 3D Electron Microscopy of Cells, University of Colorado). Binned 2k by 2k tilt series were collected on 4k by 4k charge-coupled-device Gatan camera (Gatan, Inc., Pleasanton, CA) every 1° from −70° to +70°, using the UCSF tomography or SerialEM software package (**41**). The nominal setting of defocus was −0.2 µm to −1 µm, and the pixel size of the data corresponded to 1 nm.

Cryo tomography was done on vitrious samples using a JEOL-3100 TEM equipped with an FEG operating at 300 kV; side entry goniometer (+/-70 degree tilt), liquid helium cooled stage; Gatan 2k CCD camera; and, in-column energy filter collecting every degree from -60 to +60.

Series were aligned with the help of either 10-nm or 15-nm gold fiducial markers (BBI Research, Inc., WI), and 3D reconstructed using the IMOD software package (**42**). IMOD was also used for data inspection and analysis. Where appropriate, 3D volume data were inspected interactively using the volume and surface rendering tools VOLUME ROVER (**43**) and CHIMERA **http://www.cgl.ucsf.edu/chimera**).

Time-course and time-lapse fluorescence microscopy:

For motion analysis by time-lapse microscopy, 2 µl of cells from a 2 x 10 8 cfu ml-1 32°C culture were spotted on a thin fresh 0.5CYE agar pad atop of a slide. To stain cell membranes, FM4-64 (Molecular probes) was added to CYE at a 20 µg/ml concentration. A cover slip was added immediately to cover the cells on the agar pad and the slide was analyzed by microscopy using a Nikon microscope after allowing cells 10 minutes to begin moving again. Time-lapse phase contrast images of moving cells were taken every 90seconds with a fluorescent image taken at the end of series. FM4-64 images were captured with appropriate filter sets.

Vesicle purification:

To obtain a cell free sample of vesicle structures, 25 mL batches of liquid MX cultures were added to 50mL Falcon tubes and vortexed with high agitation for 30 seconds. The vortexed cuture is then spun in a centrifuge for 10 minutes at 5000xG to pellet out the whole cells before decanting the supernatant. The liquid is next filtered through a 0.45um and then a 0.22um syringe filters to remove larger cell debris that did not pellet with previous step. Finally the cell free liquid is spun at 140000xG for one hour and the resulting pellet is resuspended in 1mL of PBS. Purification of vesicles from cells grown on agar was done exactly the same except

that before the vortexing step the samples were resuspended with a pipette into liquid CYE media.

Quantification of lipid:

Four conditions were compared in this experiment, two samples were grown in liquid CYE media with agitation to an optical density at 600 nm of 0.6 and 1.2 OD and two samples were grown on CYE agar plates for one and three days. In order to compare vesicle amounts in each sample the amounts of starting material needed to be equal. To do this pellets of the liquid culture obtained by centrifuging at 5000xg for 10 minutes were weighed and normalized with the scraped off biofilm grown on agar plates. All samples were resuspended and vesicles were purified as described above five independent times. Samples were mixed with lipid dye FM 4-64(Molecular Probes) and using a microplate(Greiner NC,USA)and plate-reader(Tecan, Vission-100 Switzerland) relative concentration of vesicle sample was determined.

In-gel Tryptic Digestion and Protein Identification:

The purified membrane vesicles were solubilized with lysis buffer and separated on a SDS-PAGE gel. Visible bands were cut from the Coomassie stained gel and subjected to tryptic digestion using a ProGest robot (DigiLab, Inc.). Briefly, the gel bands were destained and dehydrated with acetonitrile, the proteins were reduced with 10 mM DTT (60 °C, 30 min), and the reduced cysteine residues were then alkylated with 100 mM iodoacetamide (37 °C, 45 min). Prior to enzymatic digestion excess reagents were removed and the gel pieces were washed twice with 25 mM ammonium bicarbonate, dehydrated, and incubated with 250 ng sequencing grade trypsin (37 °C for 4 h). The resulting tryptic peptides were extracted from the gel with 10% formic acid as previously described (Schilling et al, 2005). The resulting peptide mixtures were analyzed by nanoLC-ESI-MSMS utilizing a 2DLC NanoLC system (Eksigent) interfaced with the LTQ XL linear ion trap mass spectrometer (ThermoFisher) equipped with the Advance Captivespray source (Michrom Bioresources). Data was searched with an in-house Mascot v2.2 search engine (Matrix Science) against a custom M. xanthus protein sequence database (downloaded from UniProt) with common contaminants appended; a reversed version was concatenated to the database to follow false discovery rate (14935 sequences; 5626671 residues). Peaklists were generated with the Mascot Daemon (Matrix Sciences) using the "ThermoFinigan LCQ/DECA RAW file" (Thermo Fisher) data import filter; search was limited to doubly- and triply-charged precursors. The following search parameters were utilized: precursor mass tolerance 0.8 Da; fragment mass tolerance 0.8 Da; tryptic digestion; 1 missed cleavage; fixed modification: Cys-carbamidomethyl; variable modifications: deamidation (Asn and Gln), Met-sulfoxide and Pyro-glu (N-term Gln).

Fluorophore-assisted carbohydrate electrophoresis for monosaccharide composition analysis:

The monosaccharide composition for the vesicle fraction was analyzed using the protocol provided by Glyko, Inc. (Hayward, CA) Briefly, neutral sugar hydrolysis was

performed by incubating 50 µl of purified vesicle fraction with 50 µl trifluoroacetic acid (4N) at 100 °C for 5 h. Amine sugars were analyzed using Hydrochloric acid (8N) at 100 °C for 1 h. On hydrolysis, the samples were dried in a centrifugal vacuum evaporator with no heat. The hydrolyzed samples were labeled overnight at 37 °C with Monosacharide labeling dye, dried and resuspended in labeling solvent for subsequent electrophoresis on a polyacrylamide gel. A Mono ladder standard for monosaccharides was run on the gel along with the hydrolyzed samples. The gel was photographed in a GelDoc (Bio-Rad, Hercules, CA)

Carbohydrate-specific lectin staining:
Wild type and EPS minus strains of *M.xanthus* cells were labeled with fluorophore conjugated derivatives of the lectin wheat germ agglutinin (WGA) (Invitrogen, Carlsbad, USA). Stock solution (1mg/ml) of Alexa 488-conjugated WGA was prepared in phosphate-buffered saline, and diluted 1:200 for the purpose of staining. Cells were allowed to adhere to poly-lysine coated microscope slide before adding a drop of the staining solution. The slides were rinsed in distilled water to remove excess stain.

FIB/SEM:
For Focused-Ion-Beam / Scanning Electron Microscopy (FIB/SEM) analysis, biofilm samples were prepared similar to HPF-resin-section TEM samples except that before HPF the samples were fixed at room temperature in a solution of 4% paraformaldehyde, 0.1% ruthenium red and 1% osmium in PBS for 30 minutes before being rinsed three times with ddH_2O and subjected to high pressure freezing. Samples were then freeze-substituted with anhydrous acetone containing 1% osmium tetroxide and 0.1% uranyl acetate and infiltrated with Epon-Araldite following established protocols. For FIB/SEM imaging we employed a Zeiss Auriga FIB/SEM workstation equipped with a Cobra Gallium column (probe size<2nm) and a Gemini electron column (probe size < 0.8nm). An energy-selective in-lens high-sensitivity backscattered-electron detector (EsB) was used for image acquisition. Slicing was achieved by using 30kV focused Ga ion beam with a probe current of 240 pA. Images were recorded after each round of ion beam milling using the SEM beam at *1.5* keV with an energy filter bias set at 750eV. Data acquisition occurred in an automated way using the ZEISS SmartSEM software, with an XY pixel size of 3 nm and Z step size of 5 nm, resulting in typical volumes of 10 µm by 8 µm by 15 µm.

References

1. Costerton J.W. (2007). The Biofilm Primer. Springer, Heidelberg. 200 pgs..

2. Sauer, K., A. K. Camper, G. D. Ehrlich, J. W. Costerton, and D. G. Davies. 2002. Pseudomonas aeruginosa displays multiple phenotypes during development as a biofilm. J. Bacteriol. 184:1140-1154.

3. Costerton, J. W., Z. Lewandowski, D. E. Caldwell, D. R. Korber, and H. M. Lappin-Scott. 1995. Microbial biofilms. Annu. Rev. Microbiol.49:711-745.

4. Hall-Stoodley, L., J. W. Costerton, and P. Stoodley. 2004. Bacterial biofilms: from the natural environment to infectious diseases. Nat. Rev. Microbiol. 2:95-108.

5. Shapiro, J. A. 1998. Thinking about bacterial populations as multicellular organisms. Annu. Rev. Microbiol. 52:81-104.

6. Costerton, J. W., P. S. Stewart, and E. P. Greenberg. 1999. Bacterial biofilms: a common cause of persistent infections. Science 284:1318-1322.

7. Beveridge, T. J. 2006. Visualizing bacterial cell walls and biofilms.Microbe 1:6.

8. Hunter, R. C., and T. J. Beveridge. 2005. High-resolution visualization of Pseudomonas aeruginosa PAO1 biofilms by freeze-substitution transmission electron microscopy. J. Bacteriol. 187:7619-7630.

9. Lawrence, J. R., D. R. Korber, B. D. Hoyle, J. W. Costerton, and D. E. Caldwell. 1991. Optical sectioning of microbial biofilms. J. Bacteriol.173:6558-6567.

10. Lawrence, J. R., G. D. Swerhone, G. G. Leppard, T. Araki, X. Zhang, M. M. West, and A. P. Hitchcock. 2003. Scanning transmission X-ray, laser scanning, and transmission electron microscopy mapping of the exopolymeric matrix of microbial biofilms. Appl. Environ. Microbiol.69:5543-5554.

11 Stoodley, P., K. Sauer, D. G. Davies, and J. W. Costerton. 2002. Biofilms as complex differentiated communities. Annu. Rev. Microbiol.56:187-209.

12. Webster, P., S. Wu, G. Gomez, M. Apicella, A. G. Plaut, and J. W. St. Geme III. 2006. Distribution of bacterial proteins in biofilms formed by non-typeable Haemophilus influenzae. J. Histochem. Cytochem.54:829-842.

13. Webster, P., S. Wu, S. Webster, K. A. Rich, and K. McDonald.2004. Ultrastructural preservation of biofilms formed by non-typeableHemophilus influenzae, p. 165-182. In M. Wilson (ed.), Biofilms 1. Cambridge University Press, Cambridge, United Kingdom

14. Graham, L. L., and T. J. Beveridge. 1990. Evaluation of freeze-substitution and conventional embedding protocols for routine electron microscopic processing of eubacteria. J. Bacteriol. 172:2141-2149.

15. Graham, L. L., R. Harris, W. Villiger, and T. J. Beveridge. 1991. Freeze-substitution of gram-negative eubacteria: general cell morphology and envelope profiles. J. Bacteriol. 173:1623-1633.

16. Hobot, J. A., E. Carlemalm, W. Villiger, and E. Kellenberger. 1984. Periplasmic gel: new concept resulting from the reinvestigation of bacterial cell envelope ultrastructure by new methods. J. Bacteriol. 160:143-152.

17. Hobot, J. A., W. Villiger, J. Escaig, M. Maeder, A. Ryter, and E. Kellenberger. 1985. Shape and fine structure of nucleoids observed on sections of ultrarapidly frozen and cryosubstituted bacteria. J. Bacteriol.162:960-971.

18. Hodgkin, J., and D. Kaiser. 1977. Cell-to-cell stimulation of movement in nonmotile mutants of *Myxococcus* . Proc. Natl. Acad. Sci. USA74:2938-2942.

19. Hartzell, P., W. Shi, and P. Youderian. 2007. Gliding motility of *Myxococcus xanthus*, p. 103-122. In D. E. Whitworth (ed.), Myxobacteria: multicellularity and differentiation. ASM Press, Washington, DC.

20. Palsdottir, H. et al., (2009). Three-dimensional macromolecular organization of cryofixed *Myxococcus xanthus* biofilms as revealed by electron microscopic tomography. J Bacteriol 191: 2077-2082.

21. Kahnt, J, Aguiluz, K., Koch, J., Treuner-Lange, A., Huntley, S., Hoppert, M., Sogaard-Andersen, L. & Hedderich, R. (2010). Profiling the outer membrane proteome during growth and development of a social bacterium *Myxococcus xanthus* by selective biotinylation and analysis of outer membrane vesicles. J. Proteome Res. 9: 5197 – 5208.

22. G.P. Dubey G.P., and Ben-Yehuda, S. (2011) Intercellular nanotubes mediate bacterial communication. Cell.144: 590-600

23. Wei, X., Pathak, D.T. & Wall, D. (2011). Heterologous protein transfer within structured myxobacteria biofilms. Mol Micro 80: 1365-2985.

24. Gorby, Y. A. et al. (2006). Electrically conductive bacterial nanowires produced by Shewanella oneidensis strain MR-1 and other microorganisms. Proc Natl Acad Sci U S A 103: 11358-11363.

25. K. D. M. Reguera, Teena Mehta, Julie S. Nicoll, Mark T. Tuominen & Derek R. Lovley, 2005. Extracellular electron transfer via microbial nanowires Nature 435 : 1098-1101

26. Miller K.R., Prescott, C.S., Jacobs, T.L. & Lassignal, N.L. (1983). Artifacts associated with quick-freezing and freeze-drying. J. Ultrastructural Res. 82: 123-133.

27. Gorby, Y., McLean, J., Korenevsky, A, Rosso, K., El-Naggar, M.Y. & Beveridge, T.J. (2008). Redox-reactive membrane vesicles produced by Shewanella. Geobiology. 6: 232 – 241.

28. Dohnalkova, A. et al. (2011). Imaging hydrated microbial extracellular polymers: comparative analysis by electron microscopy. Applied and Environmental Microbiology 77: 1254–1262.

29. Wolgemuth, C., Hoiczyk, E., Kaiser & D., Oster, G. (2002). How myxobacteria glide. Curr Biol 12: 369-377.

30. Yu, R. & Kaiser, D. (2007). Gliding motility and polarized slime secretion. Mol Microbiol 63: 454-467.

31. Arnold, J.W. & Shimkets, L.J. (1988). Cell surface properties correlated with cohesion in *Myxococcus xanthus*. Bacteriol 170: 5771-5777.

32. Behmlander, R.M. & Dworkin, M. (1991). Extracellular fibrils and contact-mediated cell interactions in *Myxococcus xanthus*. Bacteriol 173: 7810-7820.

33. Li, Y. et al. (2003). Extracellular polysaccharides mediate pilus retraction during social motility of *Myxococcus xanthus*. Proc Natl Acad Sci U S A 100: 5443-5448.

34. Rezende, E. et al. (2005)Capsular Polysaccharide Surrounds Smooth and Rugose Types of Salmonella enterica serovar Typhimurium DT104. Applied and Environmental Microbiology 71: 7345-51

35. Heymann, J. et al. (2009). 3D imaging of mammalian cells with ion-abrasion scanning electron microscopy. J Struct Biol. 166: 1-7.

36. Sanchez, C. et al. (2011). Cellular microbiology:Bacterial Networking. Nature Reviews Microbiology 9: 229.

37. Helmuth, R. & Achtman, M. (1978). Cell-cell interactions in conjugating Escherichia coli : purification of F pili with biological activity. PNAS 75: 1237–1241.

38. Mashburn, L.M. & Whiteley, M. (2005). Membrane vesicles traffic signals and facilitate group activities in a prokaryote. Nature 437: 422–425.

39. McDonald, K. L., M. Morphew, P. Verkade, and T. Muller-Reichert. 2007. Recent advances in high-pressure freezing: equipment- and specimen-loading methods. Methods Mol. Biol. 369:143–173.

40. Muller-Reichert, T., H. Hohenberg, E. T. O'Toole, and K. McDonald. 2003. Cryoimmobilization and three-dimensional visualization of C. elegans ultrastructure. J. Microsc. 212:71–80

41. Mastronarde, D. N. 2005. Automated electron microscope tomography using robust prediction of specimen movements. J. Struct. Biol. 152:36–51

42. Kremer, J. R., D. N. Mastronarde, and J. R. McIntosh. 1996. Computer visualization of three-dimensional image data using IMOD. J. Struct. Biol. 116:71–76.

43. Bajaj, C., Z. Yu, and M. Auer. 2003. Volumetric feature extraction and visualization of tomographic molecular imaging. J. Struct. Biol. 144:132–143